ORIGINAL RESEARCH

# Temperature-Sensitive Nanocarbon Hydrogel for Photothermal Therapy of Tumors

Wanlin Tan[1,2], Sijie Chen[1,2], Yan Xu[1,2], Mingyu Chen[1,2], Haiqin Liao[1,2], Chengcheng Niu [1,2]

[1]Department of Ultrasound Diagnosis, the Second Xiangya Hospital, Central South University, Changsha, Hunan, People's Republic of China; [2]Research Center of Ultrasonography, the Second Xiangya Hospital, Central South University, Changsha, Hunan, People's Republic of China

Correspondence: Chengcheng Niu, Email niuchengcheng@csu.edu.cn

**Background:** Intelligent hydrogels continue to encounter formidable obstacles in the field of cancer treatment. A wide variety of hydrogel materials have been designed for diverse purposes, but materials with satisfactory therapeutic effects are still urgently needed.

**Methods:** Here, we prepared an injectable hydrogel by means of physical crosslinking. Carbon nanoparticle suspension injection (CNSI), a sentinel lymph node imaging agent that has been widely used in the clinic, with sodium β-glycerophosphate (β-GP) were added to a temperature-sensitive chitosan (CS) hydrogel (CS/GP@CN) as an agent for photothermal therapy (PTT). After evaluating the rheological, morphological, and structural properties of the hydrogel, we used 4T1 mouse breast cancer cells and B16 melanoma cells to assess its in vitro properties. Then, we intratumorally injected the hydrogel into BALB/c tumor-bearing mice to assess the in vivo PTT effect, antitumor immune response and the number of lung metastases.

**Results:** Surprisingly, this nanocarbon hydrogel called CS/GP@CN hydrogel not only had good biocompatibility and a great PTT effect under 808nm laser irradiation but also facilitated the maturation of dendritic cells to stimulate the antitumor immune response and had an extraordinary antimetastatic effect in the lungs.

**Discussion:** Overall, this innovative temperature-sensitive nanocarbon hydrogel, which exists in a liquid state at room temperature and transforms to a gel at 37 °C, is an outstanding local delivery platform with tremendous PTT potential and broad clinical application prospects.

**Keywords:** temperature-sensitive chitosan, carbon nanoparticle suspension, photothermal therapy, hydrogels, antitumor immune response

## Introduction

Although great progress has been made in cancer research in recent years both locally and internationally, cancer is still the largest health burden worldwide.[1] Due to the high rates of cancer mortality and morbidity, more effective cancer treatments are always being sought, whether from the three traditional treatment modalities of surgery, chemotherapy and radiotherapy, or from emerging strategies, including immunotherapy, photothermal therapy (PTT), sonodynamic therapy and others, and certain achievements have been made.[2–6] Recently, designing injectable in situ hydrogels with sustained drug release have become increasingly common innovations.[7–10] Hydrogels are a three-dimensional netted polymers composed of hydrophilic polymer chains that are formed by physical or chemical crosslinking methods.[11] Hydrogels have the benefits of a soft and wet surface and a high affinity for tissue, but are a weak irritant to the body. As a result, hydrogels have exceptional biocompatibility and broad application potential in tissue engineering and sustained medication release applications.[12,13]

Intelligent response hydrogels that can sense changes in the external environment are known as environment-sensitive hydrogels, and these materials can be classified as temperature-sensitive, pH-sensitive, photosensitive and so on according to their response to different external factors.[14–17] Temperature-sensitive hydrogels have potential multifunctional applications due to their sol-gel phase transition or reversible volume change with changes in the surrounding temperature.[18–21]

**6137**

Many natural polymers can be used to prepare temperature-sensitive hydrogels, such as gelatin, chitosan (CS), and hyaluronic acid. CS is the only alkaline cationic polysaccharide found in nature. In addition to its abundant supply, simple preparation, and low price, it can be used for sterilization and to inhibit bacterial growth, reduce inflammation, stop hemorrhaging, and promote wound healing.[22–24] As a result of its ability to lower cholesterol levels, boost immunity, and eliminate toxins, as well as its high biocompatibility and rapid decomposition, CS has found widespread use in the fields of medicine and pharmacy. This drug can be loaded into hydrogels to facilitate its delivery to the site of action and then be released, which allows it to swiftly reach an appropriate concentration in the target location, show reduced loss and improved efficacy, and display fewer negative effects on normal tissue. When Sodium β-glycerophosphate (β-GP) is added to chitosan hydrogels, the mixed solution can be sensitive to temperature and remain in a solution state for an extended period at ambient temperature. Additionally, the pH value of the solution can be in the physiological pH range of the human body.[25,26] When the temperature of the hydrogel rises to 37 °C, the solution will be transformed into a gel.[27]

PTT, which uses a photothermal transduction reagent (PTA) to convert light energy into enough heat to kill tumor cells without causing damage to normal tissue under near-infrared (NIR) light irradiation, has become a promising and effective cancer treatment method with high selectivity and minimal invasiveness.[28–31] The 808nm laser, the excitation wavelength utilised in this work, is chosen from the "biological window" NIR-I (650–950 nm) in order to improve the NIR laser penetration depth, target the tumor where the PTA is located while minimizing damage to nearby normal tissue.[32,33] In recent years, it has been found that PTT not only stimulates the immune system's antitumor response but also prevents tumor metastasis.[34–37] Although increasing the laser power density and concentration of the PTA can improve the effect of PTT, a low laser power and PTA concentration are safer for clinical use, but their design still needs to be optimized.

Among all kinds of nano-biomaterials developed thus far, carbon-based nanomaterials are among the most widely studied.[38] However, previous research results are unsatisfactory because the poor dispersion and stability in aqueous solution restrict the practical applications of graphene and carbon nanotubes.[39,40] Carbon nanoparticle suspension injection (CNSI, trade name: Canarine) is the only commercially and clinically applicable carbon nanomaterial available for intratumoral injection that can dye tumor-draining lymph nodes black. CNSI has been utilized in advanced gastric cancer, breast cancer, and thyroid papillary carcinoma surgery.[41–43] At present, more than 100,000 patients receive CNSI during tumor surgery every year, and the biosafety of CNSI has been confirmed by experimental evaluations and clinical observations.[44–46] However, to our knowledge, no previous research has investigated the effect of such a clinically safe CNSI on PTT and antimetastatic cancer treatment and determined whether it activates immune responses.

The overall goal of this thesis was to design a CS/GP@CN hydrogel and explore the great potential of the clinically used sentinel lymph node imaging agent CNSI as a photothermal agent in tumor therapy in combination with a temperature-sensitive chitosan hydrogel. CNSI loaded in a hydrogel could achieve PTT under near-infrared irradiation after being administered locally into the tumor.[27] Furthermore, we highlight how a CS/GP@CN hydrogel, when subjected to PTT, enhances antitumor immune responses through dendritic cell maturation and inhibits metastasis of breast cancer cells. In summary, this innovative temperature-sensitive hydrogel with great antitumor effects has the potential in a wide range of new biomedical uses (Scheme 1).

# Materials and Methods
## Materials
Chitosan (CS, viscosity 100–200 mPa.s, deacetylation degree, ≥95%) and sodium β-glycerophosphate (β-GP, MW = 216.04 (anhydrous basis)) were purchased from Shanghai Aladdin Biochemical Technology Co., Ltd. Acetic acid was obtained from Shanghai Macklin Biochemical Technology Co., Ltd. CNSI, a commercially available imaging agent for lymph node tracing, was obtained from Chongqing Lummy Pharmaceutical Co., Ltd. The CCK-8 kit was obtained from Beyotime Biotechnology (Shanghai, China). The Calcein-AM/PI double staining kit was acquired from Yeasen Corporation (Shanghai, China). B16 and 4T1 cell lines were obtained from the Second Xiangya Hospital of Central South University (Changsha, China). All other reagents were of analytical grade and were used without further purification.
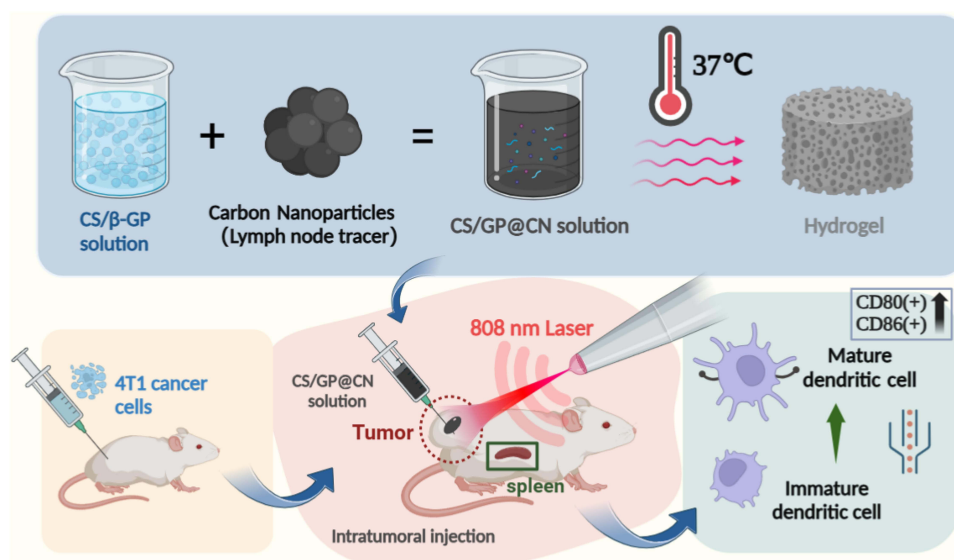
**Scheme 1** Schematic illustration of the CS/GP@CN hydrogel for PTT therapy and activating dendritic cells mature and leading to an antitumor immunity effect.

## Preparation of the CS/GP@CN Gel

To create the hydrogel, 200 mg of CS powder was thoroughly dissolved in 9 mL of 0.1 M acetic acid, and then the mixture was stirred using a magnetic bead for two hours to produce a clear CS solution.[19,27] β-GP (560 mg) was added to 1 mL of deionized water, which was maintained at 4 °C. Afterward, to make the CS/GP solution, 1 mL of the prepared β-GP solution was added to 9 mL of the CS solution in an ice bath with gentle agitation.[27] CNSI (0.3 mg/mL) was added to the CS/GP solution with agitation for 5–10 minutes to ensure even distribution. Next, the mixture was placed in a 37 °C water bath for a short period to produce the CS/GP@CN gel.

## Hydrogel Characterization

On a TA Instruments rotational rheometer with a diameter parallel plate, the rheological properties of the hydrogels were examined. The morphology of CNSI were observed using Transmission Electron Microscope (TEM) 200kv FEI Tecnai F20 (USA). Scanning electron microscopy (SEM) observations were carried out by a Tescan MIRA LMS (Czech Republic). FTIR analyses were carried out using a Fourier infrared spectrometer (Thermo Scientific iN10) in the wavenumber range 400~4000 cm$^{-1}$. A 2450 UV–vis spectrophotometer (Shimadzu, Japan) was used to acquire the ultraviolet–vis–NIR spectra.[27]

## In vitro Photothermal Performance of the CS/GP@CN Hydrogel

In a 96-well plate, PBS, CS/GP gel, and CS/GP@CN gel were separately dissolved in deionized water and exposed to an 808-nm laser (T808F2W, Minghui Optoelectronic Technology, China) for 5 minutes. Three different outputs of 0.5 W/cm$^2$, 1.0 W/cm$^2$ and 2.0 W/cm$^2$ were used in the experiment. The initial temperature in the in vitro photothermal test was approximately 25 °C.[19] The heating and cooling curves of the CS/GP@CN gel at various concentrations (0, 0.01, 0.05, 0.3 and 2 mg/mL) of CNSI were also detected. An infrared thermal imager (FLIR C2, USA) was then used to record the temperatures after certain time intervals.

## Thermal Stability and Photostability of CS/GP@CN Hydrogel

To assess the photothermal conversion efficiency (η), the wells of a 96-well plate were filled with 100 μL of CS/GP@CN hydrogels (0.3 mg/mL), which were then exposed to a 1 W/cm$^2$ laser for five minutes before cooling naturally for 15 minutes. η can be estimated using Eq. (1). S in this equation stands for the test article's surface area, hS was calculated by examining the cooling rate after the light source had been removed, Tmax denotes the hydrogel's maximum (highest)

temperature after being exposed to the 808-nm laser, and Tsurr gives the temperature in the immediate area. According to $Q_0$, heat is lost to the surrounding environment. Additionally, I (mW) is the laser power, and A($\lambda$) stands for the absorbance of the hydrogel at 808 nm. In the Supporting Information, more information is given about these calculations.[19,27]

$$\eta = \frac{(hS\ (T_{max} - T_{surr}) - Q_0)}{I\left(1 - 10^{(-A(\lambda))}\right)} \tag{1}$$

## Cell Culture
Cultures of 4T1 mouse breast cancer cells and B16 cells were maintained in RPMI (1640) medium supplemented with 10% (v/v) fetal bovine serum and 1% (v/v) penicillin–streptomycin solution at 37°C and 5% $CO_2$ with saturating humidity.

## In vitro Cytotoxicity Assay
In vitro cytotoxicity was examined with the 4T1 and B16 cell lines. Cells were cultivated for 24 h and 48 h after seeding at a density of $5 \times 10^4$ cells/well in 96-well plates (37°C, 5% $CO_2$). Then, the cells were incubated with 100 μL of fresh 10× RPMI (1640) containing CS/GP@CN hydrogels with CNSI concentrations of 0, 0.01, 0.05, 0.3 and 2 mg/mL for 24 h. Next, the cells were treated or not with three minutes of 808-nm laser irradiation at 1 W/cm². Cells treated with PBS and blank wells were employed as controls. Each test group consisted of six replicates. Then, 10 μL of CCK-8 solution was added to each well for 3 hours of incubation. A microplate reader (SpectraMax M2e) was then used to measure the OD at 450 nm.

## Apoptosis Assay
The Annexin V-APC/PI Apoptosis Detection Kit (Best Bio) was used to detect apoptosis in 4T1 and B16 cells. Cells were plated at a density of $5 \times 10^4$ cells/well in 48-well plates (37°C, 5% $CO_2$). After culture for 24 h, the cells were treated with PBS, CS/GP gel medium, or CS/GP@CN gel medium (CNSI concentration of 0.3 mg/mL) for 24 h, with or without NIR laser irradiation (808 nm, 1 W/cm², 3 min). The remaining procedures were carried out in accordance with the manufacturer's instructions. To determine the therapeutic effect, living and dead cells were stained with the reagents of the Calcein-AM/PI double staining kit and observed under a fluorescence microscope.

## Animal Models
China's Hunan Silaike Jinda Laboratory Animal Co., Ltd. supplied 4–6-week-old female BALB/c rodents. BALB/c mice were subcutaneously injected with 100 μL of serum-free cell medium containing $1 \times 10^6$ 4T1 cells to produce mice with 4T1 breast tumors. All animal experiments were approved by the Ethics Committee of the Second Xiangya Hospital of Central South University and conducted in accordance with the guidelines of the Central South University Department of Laboratory Animals.

## In vivo Antitumor Effect and Activated Antitumor Immune Response
When the tumor size reached approximately 100 mm3, mice were randomly divided into five groups: (1) saline, (2) laser only, (3) CS/GP gel, (4) CS/GP@CN gel (CNSI concentration of 0.3 mg/mL), and (5) CS/GP@CN gel (CNSI concentration of 0.3 mg/mL) + laser. After intratumoral injection of 100 μL of saline, CS/GP gel, or CS/GP@CN gel (CNSI concentration of 0.3 mg/mL) into the appropriate group of mice, the tumor sites of groups 2 and 5 were exposed to an 808-nm laser (1.0 W/cm², 10 min). Mouse temperatures were measured and infrared images were acquired. Tumor size and body weight were measured every two days for 18 days, and the following formula was used to calculate tumor volume: length × width × width/2. Every day, photographs of the tumor sites were taken to track the therapeutic effect of the therapy. At the end of the study, the mice were killed, and the tumors were extracted for H&E, Ki67, and TUNEL staining. H&E staining was used to examine the heart, liver, spleen, lung, kidney, and tumor under an optical microscope.

To assess the immune responses elicited by antitumor PTT, each mouse's spleen was collected and stained with anti-CD80-PE, anti-CD86-APC, and anti-CD11c-FITC antibodies according to the manufacturer's protocols before being evaluated by flow cytometry.

## Assessment of Lung Metastasis

Ex vivo assessment of lung tissues was performed to evaluate lung metastasis following PTT with CS/GP@CN gel. Mice afflicted with tumors were arbitrarily split into five groups (n = 4 in each group): (1) saline, (2) laser only, (3) CS/GP gel, (4) CS/GP@CN gel (CNSI concentration of 0.3 mg/mL), and (5) CS/GP@CN gel (CNSI concentration of 0.3 mg/mL) + laser. The therapies were identical to the antitumor therapies mentioned previously. On day 35 following the initial treatment, all lungs were extracted. Metastatic lesions, which appeared as white nodules on the surface of the lungs, were enumerated and stained with H&E.

## Statistical Analysis

All data is displayed as the means ± SD. One-way ANOVA and Student's *t*-test were used for data analysis (Origin 2022 software). A value of *$p$ <0.05 was considered statistically significant.

# Results and Discussion
## Preparation and Characterization of the CS/GP@CN Hydrogels

Because of the enhanced hydrogen bonding, electrostatic attraction, and hydrophobic interactions between CS and β-GP, it was possible to successfully produce the CS/GP@CN hydrogel. At ambient temperature, both the CS/GP solution and the CS/GP@CN solution were flowable and did not solidify; however, upon heating to 37 °C, a typical solid-state hydrogel formed, regardless of whether CNSI was added. This is depicted in Figure 1A. By dissolving CNSI and β-GP in CS solution, it was possible to generate a homogenous CS/GP@CN solution that stayed in a liquid state and could be easily transferred to a 1 mL syringe and pushed out below body temperature (Figure 1B and C). This solution was prepared because it remained in a liquid form throughout the preparation process. Moreover, this suggests that CNSI does not influence the injectability of the CS solution when it is at room temperature.

The morphology of CNSI and the CS/GP@CN gel was studied using transmission electron microscopy (TEM) and scanning electron microscopy (SEM). CNSI exhibited beaded aggregation behavior and a consistent particle size of 100 nm (200 kv) with a smooth and spherical appearance (Figure 1D and E). Impressively, the stable and condensed three-dimensional network structures of the novel hydrogel are clearly observed in Figure 1F.

To investigate the biomechanical features of the gel, its G′ and G″, which represent the storage modulus and loss modulus, respectively, were analyzed and compared. The geometry of the temperature-sensitive chitosan hydrogel was determined after the temperature hit the gelation temperature, where G′ = G″. The temperature at which the CS/GP hydrogel gelated was approximately 37 °C, as shown in Figure 1G. The gelation time indicates the hydrogel's strength and gelation rate. The gelation time is determined by the temperature at which G′ is greater than G″ during the process of gelation. Dynamic time scanning experiments were carried out with the hydrogel precursor solutions at the same temperature as the human body (37 °C). According to Figure 1H, the amount of time required for the CS/GP hydrogel to form was approximately one hundred seconds. This new hydrogel is thus an amazing injectable material for local in vivo administration, as it possesses exceptional mechanical characteristics.[27]

As shown in Figure 1I, comparing the infrared spectra of the CS powder, β-GP and the CS/GP hydrogel (after freeze-drying), 1562 cm-[1] and 1410 cm-[1] in hydrogel correspond to the characteristic absorption peaks of bending vibration of N-H and C-H in CS, respectively, indicating the presence of CS in the hydrogel. Additionally, the peaks at 1132 cm-[1], 1057 cm-[1] and 967 cm-[1] correspond to the Antisymmetric stretching vibration and Symmetrical stretching vibration of $PO_4^{3-}$ in β-GP, indicating that β-GP also exists in the hydrogel. Moreover, the positions and shapes of the O-H and N-H absorption peaks of at 3223 cm-[1] in the hydrogel spectrum are quite different from those corresponding peaks in the β-GP and CS spectra, indicating the hydrogen bonds that N-H and P-O formed in the hydrogel results in peak shift. The shift in the N-H peak of CS from 1598 cm-[1] to 1652 cm-[1] in the CS/GP hydrogel spectrum also indicates that the
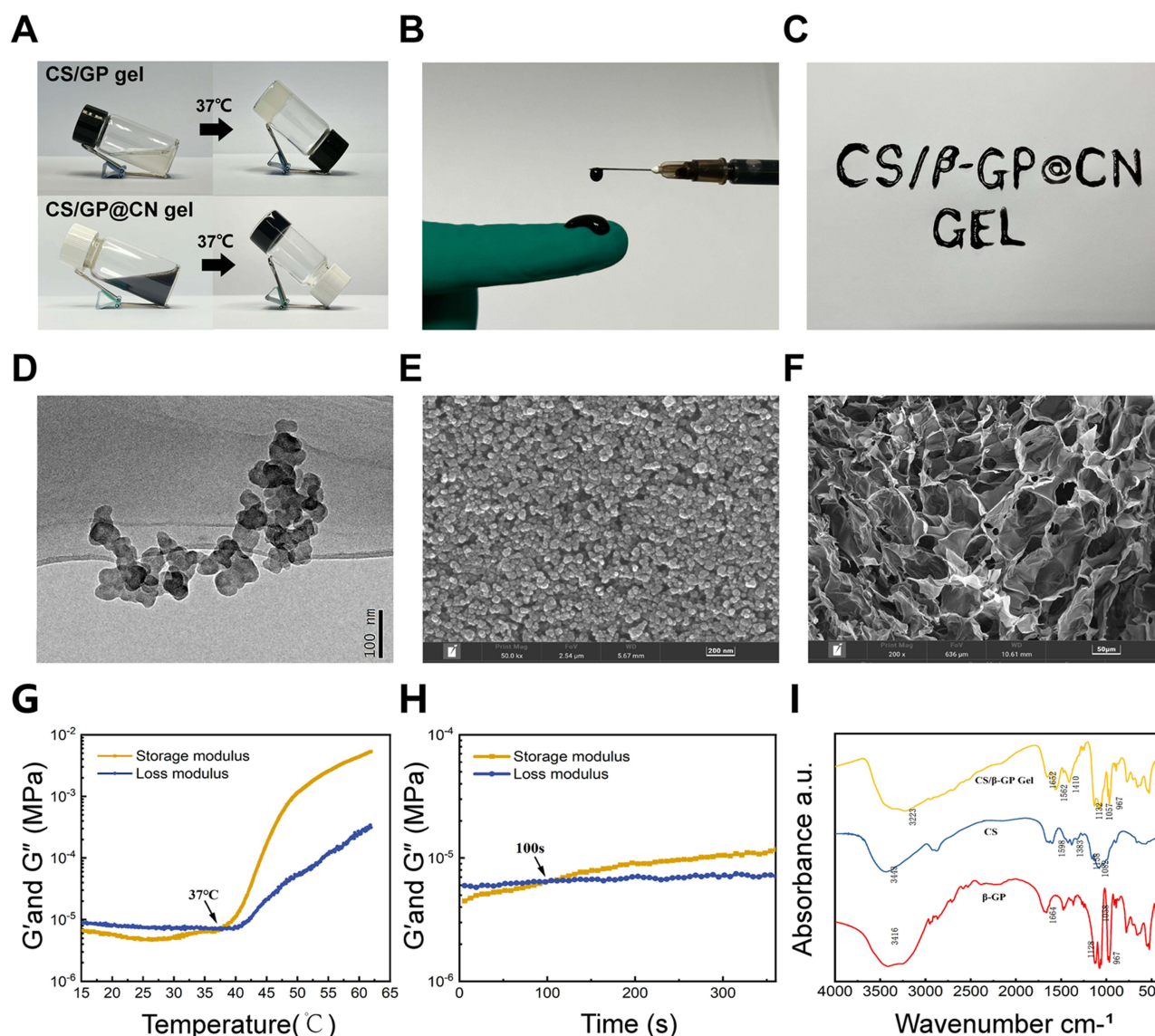
**Figure 1** Characterization of hydrogels. (**A**) Photographs of the gelation behavior of Gel at 37 °C. (**B**) and (**C**) Photographs of injectable property in vitro. (**D**)TEM image of CNSI (scale bar = 100 nm). SEM images focused on the cross-section of (**E**) CNSI (scale bar = 200 nm) and (**F**) CS/GP@CN Gel (scale bar = 50 μm). (**G**) The dynamic temperature sweep tests and (**H**) the dynamic time sweep tests of CS/GP Gel. (**I**) The FTIR spectra of CS/GP Gel.

N-H bond participates in hydrogen bonding. In summary, the P-O group in β-GP will form hydrogen bonds with the N-H moiety in CS to form a CS/GP hydrogel.[47,48]

## In vitro Photothermal Performance of the CS/GP@CN Hydrogel

To evaluate its photothermal performance, the CS/GP@CN hydrogel was exposed to laser irradiation at 808 nm (1.0 W/cm$^2$, 5 min). As indicated in Figure 2A, after 5 minutes of irradiation, the temperatures in the free CN and CS/GP@CN gel groups rose by 30 °C, whereas the rise in temperature in the control group (PBS) was only approximately 1 °C.[27] As a result, the photothermal impact of CN in the hydrogel was greatly preserved, and the CS/GP@CN gel is capable of efficiently converting 808-nm NIR laser energy into heat due to its strong absorption in the NIR region.

Once the concentration of CNSI was increased to 0.05 mg/mL, 0.30 mg/mL and 2.00 mg/mL, the temperature of the hydrogel after irradiation at the same power density of 1.0 W/cm$^2$ increased to approximately 54.00 °C, 60.2 °C and 64.7 °C, respectively within 5 min (Figure 2B). At a CNSI concentration of 0.30 mg/mL in the gel, the CS/GP@CN gel was irradiated with three different laser power densities (0.5 W/cm$^2$, 1 W/cm$^2$ and 2 W/cm$^2$) for five minutes, and the
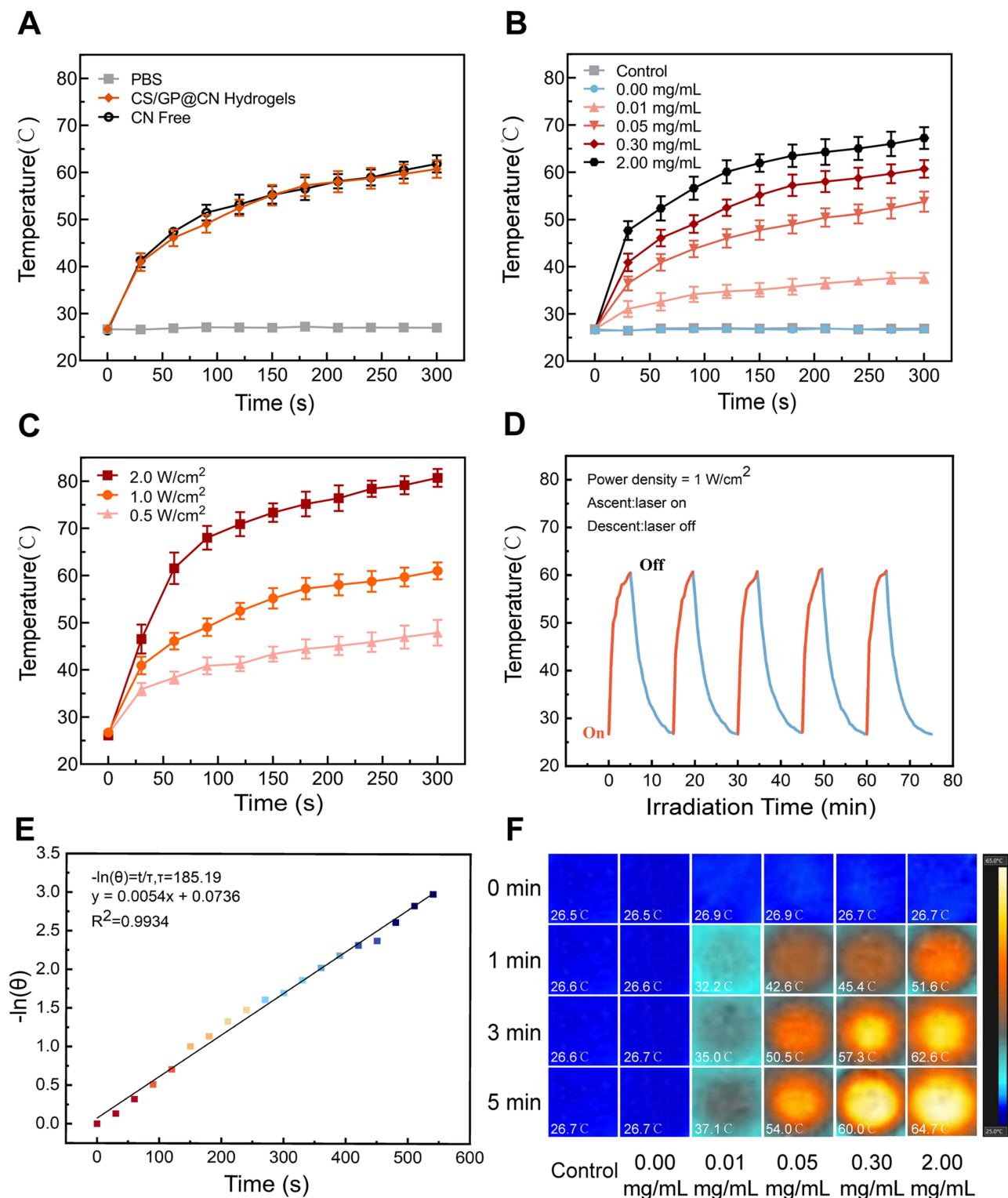
**Figure 2** In vitro photothermal performance of CS/GP@CN Gel. (**A**) Temperature changes of PBS, CN-free, CS/GP@CN Gel under irradiation at 808 nm (1.0 W/cm², 5min). (**B**) Temperature changes of different concentration of CNSI in CS/GP@CN Gel under irradiation at 808 nm (1.0 W/cm², 5min). (**C**)Temperature changes of CS/GP@CN Gel under irradiation with three different density of laser power (0.5 W/cm², 1 W/cm² and 2 W/cm²). (**D**) Photostability of CS/GP@CN Gel under 808-nm laser irradiation (1 W/cm²). (**E**) The linear regression curve of the temperature cooling time (t) vs - ln(θ) of CS/GP@CN Gel. (**F**) Representative thermographic images of different concentration of CNSI in CS/GP@CN Gel under irradiation at 808 nm (1.0 W/cm², 5min).

temperature of the hydrogel rose to 46.90 °C, 60.20 °C and 79.90 °C, respectively (Figure 2C). Based on the above findings, when the power density was 1.0 W/cm$^2$ and the concentration of CNSI in the gel is 0.30 mg/mL, the photothermal performance of the gel can serve its purpose.

Then, 5 laser ON/OFF cycles were performed to evaluate the photostability of the CS/GP@CN hydrogel (Figure 2D). The temperature increases of the CS/GP@CN hydrogel after 5 laser ON/OFF cycles were 35.3 °C, 35.6 °C, 37.2 °C, 34.2 °C and 35.9 °C, indicating that the CS/GP@CN hydrogel possesses reliable and efficient PTT characteristics after five laser irradiation ON/OFF cycles. When comparing our results to those of previous studies that used IR780 and ICG as PTA,[49] it must be pointed out that our "black gel" shows incredibly tiny temperature variations after the same amount of cycles because of the strong photothermal stability of CNSI. Consequently, the outstanding photostability of the CS/ GP@CN hydrogel makes it a promising PTT system for fighting cancer.

The temperature cooling time linear regression curve (t) vs - ln(θ) of the CS/GP@CN gel at a CNSI concentration of 0.3 mg/mL and irradiation parameter of 808-nm at 1 W/cm$^2$ is shown in Figure 2E. The photothermal conversion efficiency (η) value and time constant (τs), which refers to the heat transfer of the CS/GP@CN hydrogel at 808 nm, were calculated to be 58.51% and 185.19 s, respectively (see the calculation equations in the Supporting Information). The photothermal conversion efficiency (η) value of this study are substantially better than that of the magnetic hollow porous carbon NPs designed by Wu et al(36%)[50] and of the CMD gel system prepared by Zheng et al (both in NIR I 22.18% vs 22.34% and NIR II 31.42% vs 35.44% bio-windows).[19]

As shown in Figure 2F, the CS/GP hydrogel group that CNSI concentration of 0.00 mg/mL did not produce a significant temperature increase after laser irradiation, similar to the group that PBS as the blank control, due to the absence of a photothermal agent.

Large absorption coefficients and high photothermal conversion efficiencies indicate that CNSI, which exhibits structural properties similar to those of other carbon nanomaterials, has similar photothermal conversion capabilities for tumor PTT applications and indicates that this novel hydrogel has additional prospects in the medical field.

## In vitro Cellular Experiments

After 24 and 48 hours of incubation with B16 (mouse melanoma) and 4T1 (mouse breast cancer) cells, the hydrogel extracts exhibited negligible cytotoxicity (Figure 3A). The activity of the tumor cells exceeded 95% at all times tested. Additional cell experiments were conducted to investigate the PTT effect of the hydrogels.[27] Impressively, as shown in Figure 3B and C, the viability of the cells treated with PBS or CS/GP gel medium with or without NIR laser irradiation (808 nm, 1 W/cm$^2$, 3 min) was far beyond 95% in both B16 and 4T1 cells, demonstrating that laser irradiation alone was incapable of killing 4T1 cells. In stark contrast, the viability of the cells treated with the CS/GP@CN gel medium with CNSI concentrations of 0.05 mg/mL, 0.30 mg/mL and 2.00 mg/mL and irradiation parameters of 808-nm and 1.0 W/cm$^2$ decreased significantly 55.84%, 26.75% and 16.78% in B16 cells and 84.60%, 66.36% and 16.57% in 4T1 cells. Not withstanding its limitation namely there is certain difference in the viability after the PTT treatment between the B16 and 4T1 cell lines in the In vitro cellular experiments, these results do suggest that our black gel could be able to kill tumor cells successfully and even more efficiently compared to those of other studies.[19,27]

We also separately stained living and nonliving cells with calcein (green fluorescence) and PI (red fluorescence). In line with the CCK-8 assay results, the Calcein/PI staining results revealed that few of the cells incubated with saline and the CS/GP@CN gel died, whereas a large quantity of cells treated with the CS/GP@CN gel and three minutes of 808-nm laser irradiation were killed, demonstrating a significant decrease in cell viability as shown by the red fluorescence signal (Figure 3D). This could not be noticed from cells treated with PBS, laser only, and the CS/GP gel, further indicating that our black gel can efficiently kill tumor cells. On the basis of the above results, it was known that CS/GP@CN gel has exceptional in vivo biocompatibility, demonstrating that this innovative hydrogel possesses the capability to load various water-soluble medicines for controlled release. Thus, this hydrogel provides a great platform for local anticancer therapy, such as immunotherapy, PTT, or combination therapy.

## In Vivo Antitumor Effect and Activated Antitumor Immune Response

The PTT antitumor effects of the hydrogels were monitored in 4T1 tumor-bearing mice that were randomly divided into five groups: (1) saline, (2) laser only, (3) CS/GP gel, (4) CS/GP@CN gel (CNSI concentration of 0.3 mg/mL), and (5)
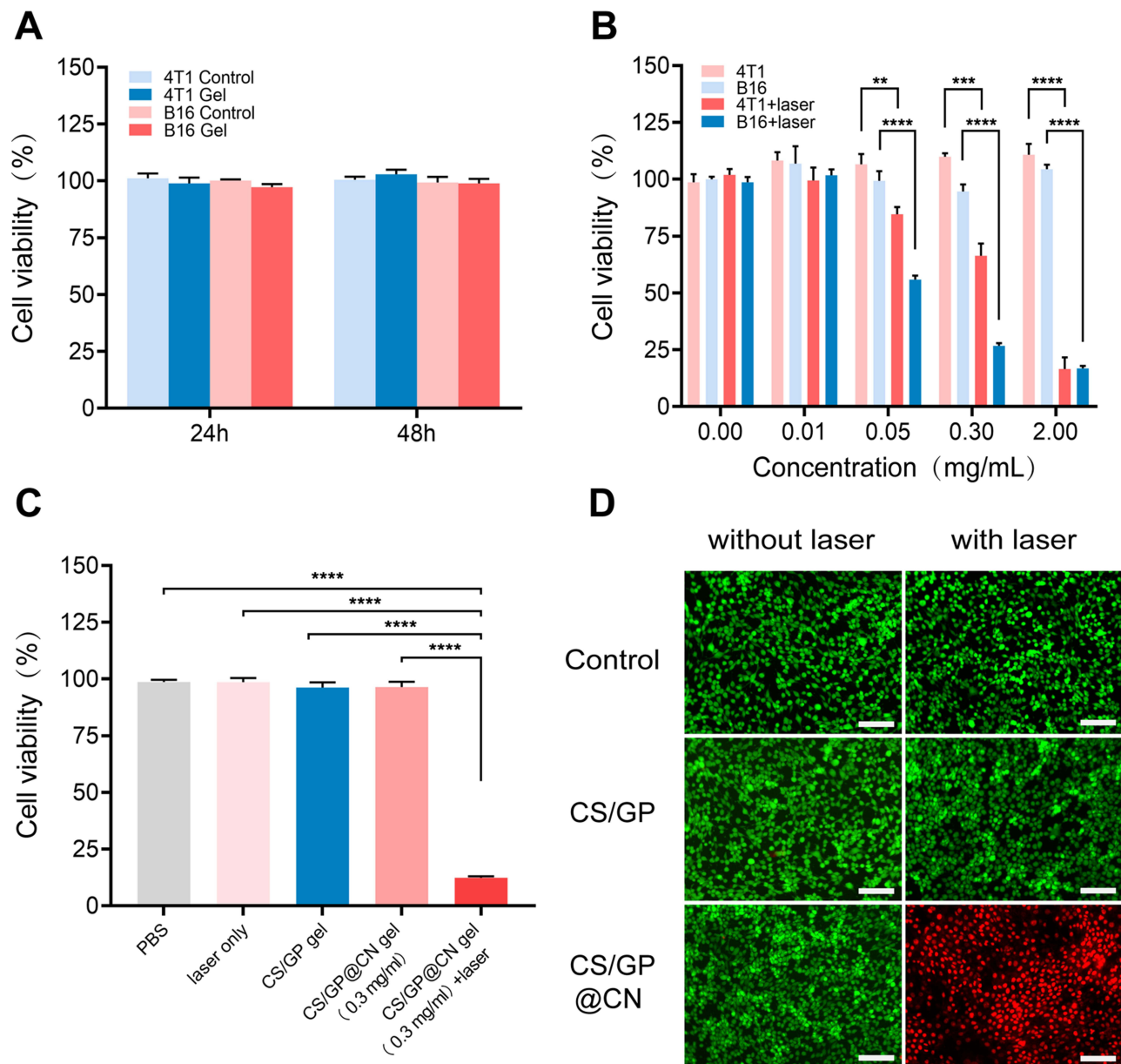
**Figure 3** In vitro cytotoxicity and photothermal therapy effect. (**A**) CCK-8 assays of B16 and 4T1 cells after incubation with CS/GP@CN Gel for 24h and 48h. (**B**)Relative viabilities of B16 and 4T1 cells after incubation with different concentrations of CS/GP@CN Gel and subsequent exposure to 808-nm light at a power density of 0.3 W/cm$^2$ for 3 min. (**C**) Cell viability of 4T1 cells after different treatments (**p<0.01, ***p<0.001, ****p<0.0001) (**D**)Confocal images of Calcein AM/PI-stained 4T1 cancer cells after incubation after different treatments. Scale bar: 200 μm.

CS/GP@CN gel (CNSI concentration of 0.3 mg/mL) + laser. On a daily basis for 18 days following intratumoral injection, the tumor volume and body weight of the rodents were observed and recorded. Infrared thermal photographs of the mice are shown in Figure 4A. The final temperature in the saline group reached 27.8 °C, whereas that in the CS/GP@CN gel + laser group was 57.1 °C, indicating that the CS/GP@CN gel could absorb NIR light and convert it into heat energy in tumors. Surely, 57.1°C is sufficient to kill the cancer cells and this is in accord with earlier studies that as a result of protein denaturation, cancer cells will be irrevocably damaged by elevated temperatures after laser for a certain time and lead to apoptosis (≤45°C) or necrosis (>50°C).[32,51,52]

Excellent antitumor effects were clearly seen in the 5 groups after various treatment approaches (Figure 4B-D). Tumors from the first four groups continued to grow at a similar rate, indicating that saline, laser only, the CS/GP gel or the CS/GP@CN gel without laser irradiation did not have antitumor effects. In contrast, as expected, the CS/GP@CN gel
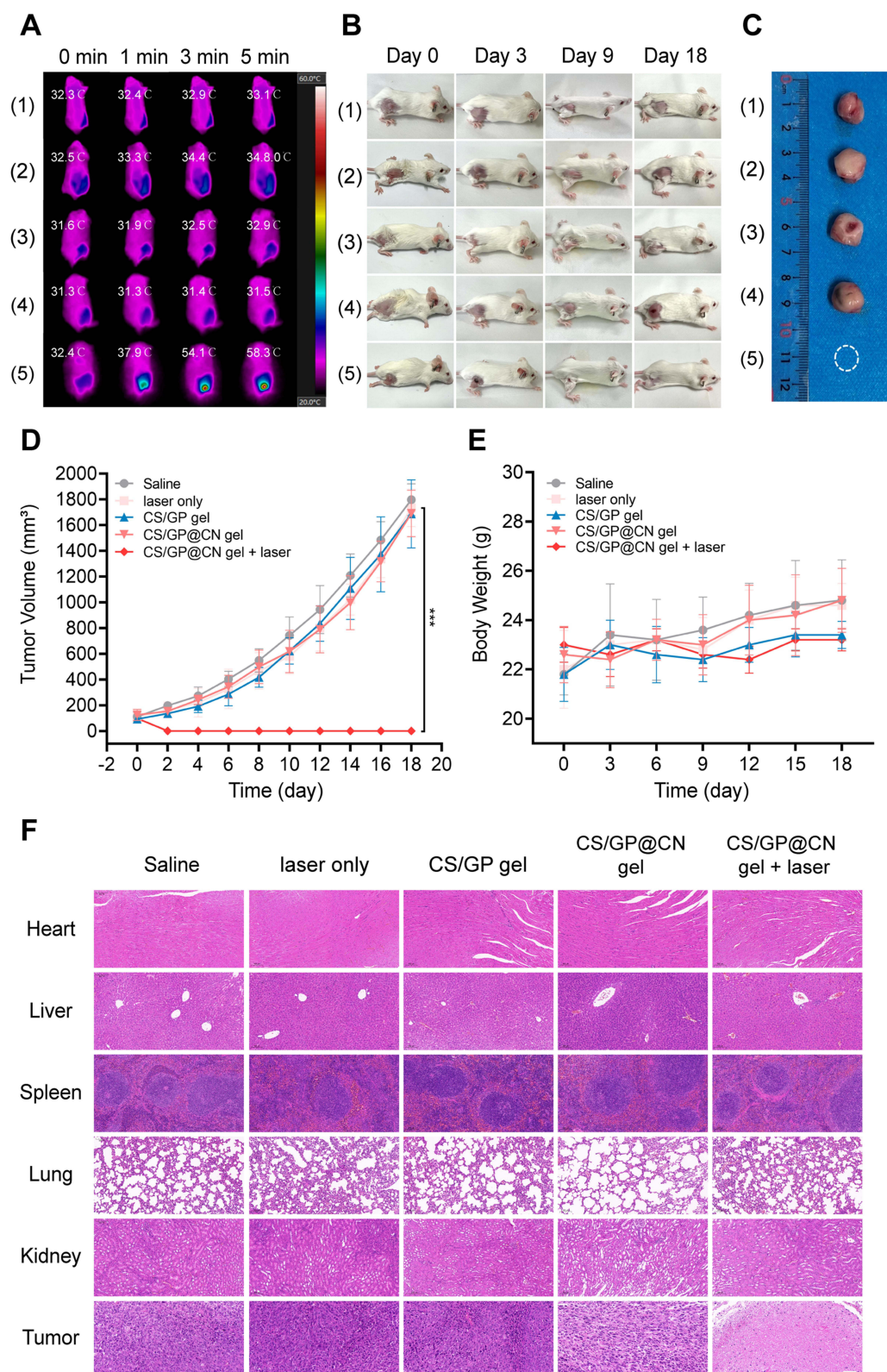
**Figure 4** In vivo antitumor therapy. (**A**) Infrared thermal images of tumor-bearing mice with different treatments: (1) saline, (2) laser only, (3) CS/GP gel, (4) CS/GP@CN gel (CNSI of 0.3 mg/mL), (5) CS/GP@CN gel (CNSI of 0.3 mg/mL) +laser. (808 nm, 1 W/cm², within the first 5 min). (**B**) Photographs of 4T1 tumor-bearing mice in each group. (**C**) Photographs of tumors after different treatments. (**D**) Tumor growth curve after different treatments (*p<0.05). (**E**) Body weight of mice after different treatments (***p<0.001). (**F**) H&E staining of lungs, livers, spleens, kidneys, hearts and tumor tissue slices after different treatments, scale bar = 100μm.

+ laser treatment group exhibited evident growth restraint and the tumors were efficiently destroyed (p<0.05) because of the photothermal effect of CNSI. On day 18, there were no remaining hydrogels in the subcutaneous tissue of the rodents in the CS/GP@CN gel + laser group. In addition, the body weights of the rodents in each group did not decrease significantly during the various treatments (Figure 4E).

The mice were sacrificed after 18 days, and their organs were subjected to tissue H&E staining and immunofluorescence staining analyses. The H&E staining images of the tumors in the 5th group (CS/GP@CN gel group) after PTT showed severe cellular destruction and coagulation necrosis (Figure 4F). H&E staining analysis of the hearts, livers, spleens, lungs and kidneys of the mice demonstrated no evident damage, inflammation or lesions, indicating that our "black gel" system has few negative effects on normal tissues and possesses in vivo biocompatibility, safety, and antitumor efficacy.

Importantly, the fewest proliferating cells with green fluorescence in the Ki67 assays (1.00±0.00%) and the greatest number of necrotic cells exhibiting green fluorescence in the TUNEL assays (84.33±3.06%) were found after treatment with CS/GP@CN
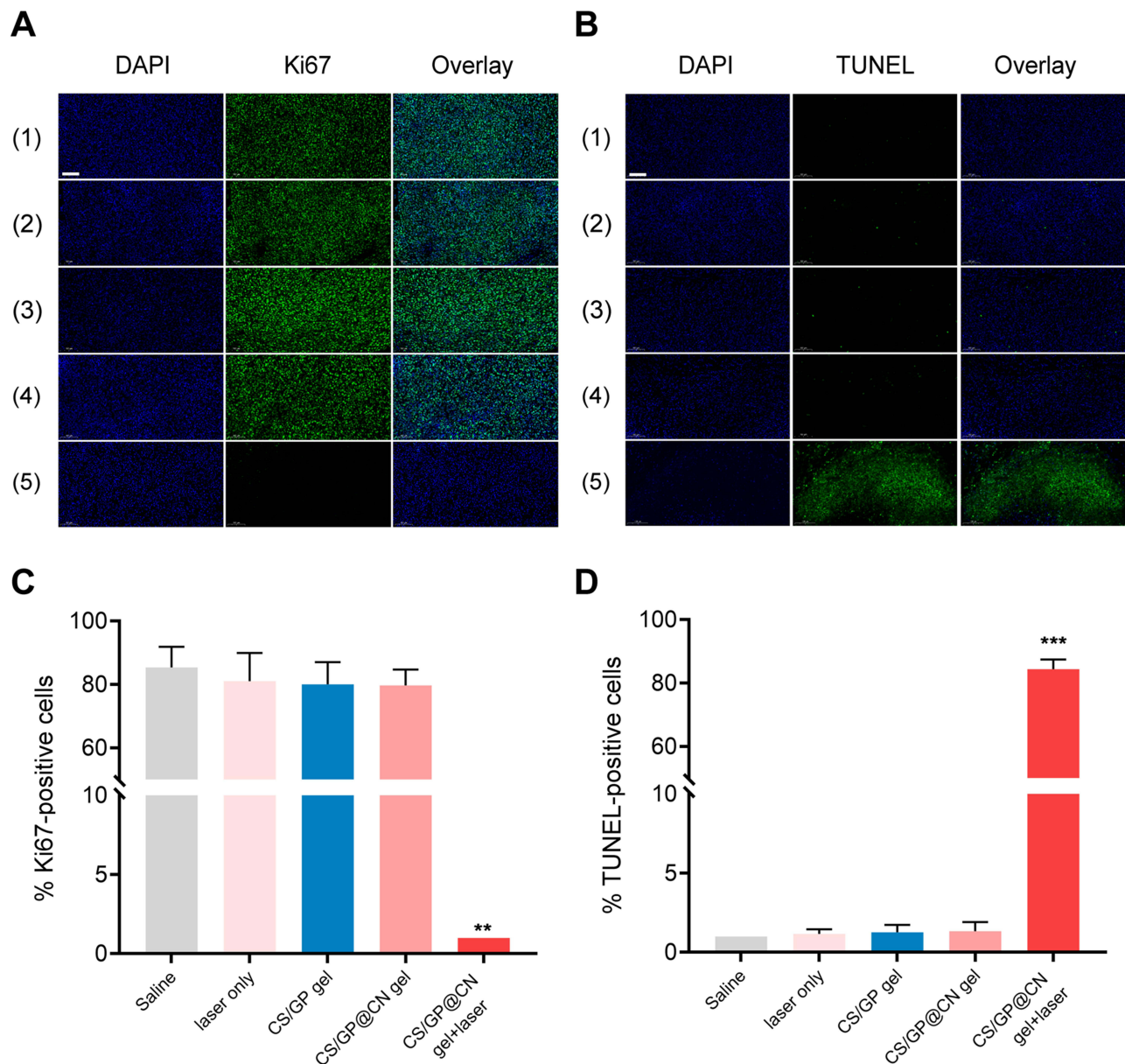


Figure 5 (**A**) Ki67 and (**B**) TUNEL of tumor tissue slices after different treatments: (1) saline, (2) laser only, (3) CS/GP gel, (4) CS/GP@CN gel (CNSI of 0.3 mg/mL), (5) CS/GP@CN gel (CNSI of 0.3 mg/mL) +laser. (808 nm, 1 W/cm², 3 min), scale bar = 100 μm. (**C**) Relative Ki67-positive cells and (**D**) TUNEL-positive cells in tumor tissues after different treatments (**p<0.01, ***p<0.001).

gel and 808-nm NIR irradiation compared with the other groups (Figure 5), demonstrating that the CS/GP@CN gel combined with PTT could effectively inhibit the development of tumor cells and successfully accelerate tumor cell apoptosis.
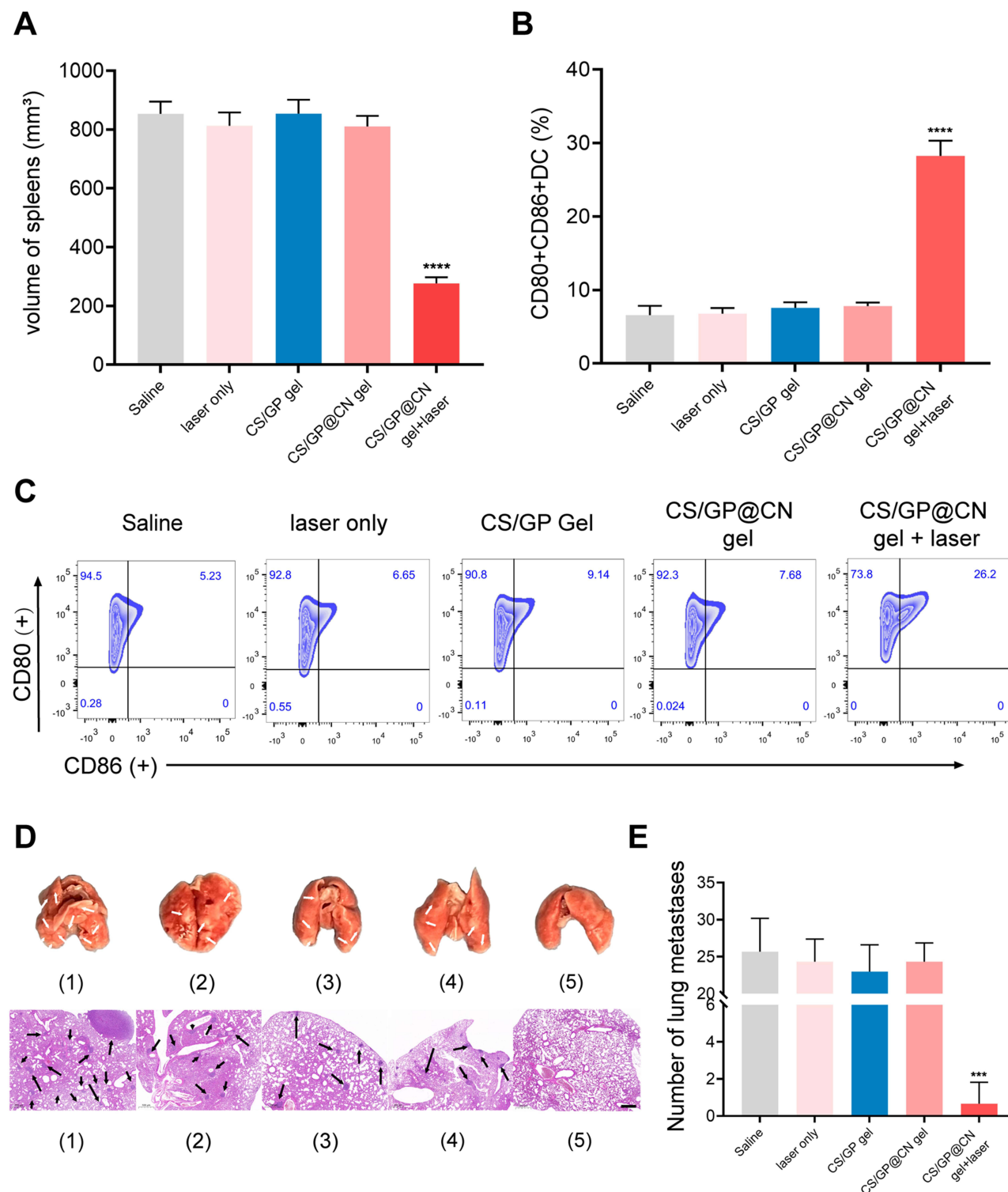


Figure 6 (**A**) volume of spleens obtained from mice in different treatment groups. (**B**) Quantification of CD80 and CD86 expression and (**C**) representative FACS plots on dendritic cells gated by CD11c+ cells. (**D**) General Photographs of lungs and H&E-stained lung sections from 4T1 tumor-bearing mice after indicated treatments on day 35. Tumor metastases in the H&E stained lung slices are indicated by black arrows. Scale bar = 500 μm. (**E**) Quantitative analysis of tumor metastases in the H&E stained lung slices (***p<0.001, ****p<0.0001).

Dendritic cells in the spleens were examined on day 21 to evaluate the immune responses that were produced by the antitumor PTA. As shown in Figure 6A, the spleen volume in the CS/GP@CN gel + laser group was much lower than that in the other groups. Moreover, as shown in Figure 6B and C, the percentage of mature dendritic cells (CD11c+CD80 +CD86+) in the CS/GP@CN gel + laser group was approximately 26.2%, which was notably higher than that in the other groups. These results demonstrated that, as expected, when combined with PTT, the CS/GP@CN gel had the ability to trigger antitumor immune responses to a certain degree. The antitumor immune responses that were produced by CS/ GP@CN gel with PTT could, to some extent, be further improved by the production of more mature dendritic cells.

Finally, due to the high lung metastasis in 4T1 tumor-bearing mice, the antimetastatic impact of CS/GP@CN gel was studied in these animals.[49] Representative gross inspections and H&E staining of the lung metastatic lesions in each of the four groups are shown in Figure 6D and E, respectively. On day 21 following therapy, obvious metastatic lesions were seen in the lungs of the animals in the saline group, where the average number of tumors was 25.67±4.51. When exposed to laser only, CS/GP gel or CS/GP@CN gel, the average number of tumors in the lungs was 24.33±3.06 (laser only group), 23.00±3.61 (CS/GP gel group), or 24.33±2.52 (CS/GP@CN gel group). When PTT treatment was administered, the average number of tumors in the lungs sharply decreased to 0.67±1.16 (CS/GP@CN gel + laser group). Clearly, the mice in the CS/GP@CN gel + laser group had fewer tumors overall than those in the other groups (p<0.05). In particular, three of the animals developed extremely small metastatic lesions in their lungs. These findings suggested that PTT with the CS/GP@CN gel produced substantial antimetastatic effects in the lungs; with the help of PTT, the CS/GP@CN gel nearly averted lung tumor metastasis.

## Conclusion

Herein, a local delivery system for tumor therapy that is both injectable and temperature-sensitive with good biocompatibility was developed. The phototoxicity effect of the CS/GP@CN hydrogel was tested on cancer cells as well as mice to determine whether it was feasible. The inclusion of the photothermal material CNSI led to the development of multifunctional in vivo tumor PTT with high photothermal conversion efficiency. Moreover, the CS/GP@CN hydrogel combined with PTT could stimulate the antitumor immune response and significantly reduce tumor lung metastasis. In the future, we plan to improve this method by loading multifunctional drugs (eg, antineoplastic and immunomodulating agents) to achieve treatment that is both very effective and integrated for breast cancer and to overcome the issues of novel hydrogels (eg, techniques for pharmacokinetics, biodistribution and drug delivery route optimization). Thus, this study of the CS/GP@CN hydrogel has great potential for on-demand and continuous drug delivery and lays the groundwork for future research into future clinical applications.

## Data Sharing Statement

The original contributions presented in the study are included in the article/Supplementary Material. Further inquiries can be directed to the corresponding author.

## Author Contributions

CN contributed to the conception and design of the work. WT participated to data analysis and manuscript writing. SC, YX, MC and HL participated to data collection. All authors made a significant contribution to the work reported, whether that is in the conception, study design, execution, acquisition of data, analysis and interpretation, or in all these areas; took part in drafting, revising or critically reviewing the article; gave final approval of the version to be published; have agreed on the journal to which the article has been submitted; and agree to be accountable for all aspects of the work.

## Funding

# Disclosure

All authors have no conflicts of interest to disclose for this work.

# References

1. Siegel RL, Miller KD, Wagle NS, Jemal A. Cancer statistics, 2023. *CA Cancer J Clin*. 2023. doi:10.3322/caac.21763
2. Zhen W, Weichselbaum RR, Lin W. Nanoparticle-Mediated Radiotherapy Remodels the Tumor Microenvironment to Enhance Antitumor Efficacy. *Adv Materials*. 2023;35(21). doi:10.1002/adma.202206370
3. Teng H, Wang Y, Sui X, et al. Gut microbiota-mediated nucleotide synthesis attenuates the response to neoadjuvant chemoradiotherapy in rectal cancer. *Cancer Cell*. 2023;41(1):124–138.e6. doi:10.1016/j.ccell.2022.11.013
4. Bueno-Muiño C, Echavarría I, López-Tarruella S, et al. Assessment of a Genomic Assay in Patients With ERBB2 -Positive Breast Cancer Following Neoadjuvant Trastuzumab-Based Chemotherapy With or Without Pertuzumab. *JAMA oncol*. 2023;9(6):841. doi:10.1001/jamaoncol.2023.0187
5. Guo K, Jiao Z, Zhao X, Hu Y, Zhao N, Xu FJ. Melanin-Based Immunoregulatory Nanohybrids Enhance Antitumor Immune Responses in Breast Cancer Mouse Model. *ACS nano*. 2023;17(11):10792–10805. doi:10.1021/acsnano.3c02287
6. Zhang C, Pu K. Organic Sonodynamic Materials for Combination Cancer Immunotherapy. *Adv Materials*. 2023. doi:10.1002/adma.202303059
7. Li G, Liu S, Chen Y, et al. An injectable liposome-anchored teriparatide incorporated gallic acid-grafted gelatin hydrogel for osteoarthritis treatment. *Nat Commun*. 2023. doi:10.1038/s41467-023-38597-0
8. Sharma R, Yadav S, Yadav V, et al. Recent advances in lipid-based long-acting injectable depot formulations. *Adv Drug Deliv Rev*. 2023;199:114901. doi:10.1016/j.addr.2023.114901
9. Wu S, Zhang H, Wang S, et al. Ultrasound-triggered in situ gelation with ROS-controlled drug release for cartilage repair. *Mater Horizons*. 2023;10 (9):3507–3522. doi:10.1039/d3mh00042g
10. Zhang Y, Shi K, Yang X, et al. Sustained release of levobupivacaine from temperature-sensitive injectable hydrogel for long-term local anesthesia in postoperative pain management. *Biomaterials*. 2023. doi:10.1016/j.biomaterials.2023.122129
11. Cao H, Duan L, Zhang Y, Cao J, Zhang K. Current hydrogel advances in physicochemical and biological response-driven biomedical application diversity. *Signal Transduction Targeted Therapy*. 2021;6(1). doi:10.1038/s41392-021-00830-x
12. Oliva N, Conde J, Wang K, Artzi N. Designing Hydrogels for On-Demand Therapy. *Acc Chem Res*. 2017;50(4):669–679. doi:10.1021/acs.accounts.6b00536
13. Liang Y, He J, Guo B. Functional Hydrogels as Wound Dressing to Enhance Wound Healing. *ACS nano*. 2021;15(8):12687–12722. doi:10.1021/acsnano.1c04206
14. Miyata T, Uragami T, Nakamae K. Biomolecule-sensitive hydrogels. *Adv Drug Deliv Rev*. 2002;54(1):79–98. doi:10.1016/s0169-409x(01)00241-1
15. Abune L, Wang Y. Affinity Hydrogels for Protein Delivery. *Trends Pharmacol Sci*. 2021;42(4):300–312. doi:10.1016/j.tips.2021.01.005
16. Yang X, Zhang C, Deng D, Gu Y, Wang H, Zhong Q. Multiple Stimuli-Responsive MXene-Based Hydrogel as Intelligent Drug Delivery Carriers for Deep Chronic Wound Healing. *Small*. 2022. doi:10.1002/smll.202104368
17. Zong S, Wen H, Lv H, et al. Intelligent hydrogel with both redox and thermo-response based on cellulose nanofiber for controlled drug delivery. *Carbohydr Polym*. 2022;278. doi:10.1016/j.carbpol.2021.118943
18. Zhou W, Duan Z, Zhao J, Fu R, Zhu C, Fan D. Glucose and MMP-9 dual-responsive hydrogel with temperature sensitive self-adaptive shape and controlled drug release accelerates diabetic wound healing. *Bioactive Materials*. 2022. doi:10.1016/j.bioactmat.2022.01.004
19. Zheng Y, Wang W, Zhao J, et al. Preparation of injectable temperature-sensitive chitosan-based hydrogel for combined hyperthermia and chemotherapy of colon cancer. *Carbohydr Polym*. 2019;222:115039. doi:10.1016/j.carbpol.2019.115039
20. Li Z, Huang J, Jiang Y, et al. Novel Temperature-Sensitive Hydrogel Promotes Wound Healing Through YAP and MEK-Mediated Mechanosensitivity. *Adv Healthcare Mater*. 2022. doi:10.1002/adhm.202201878
21. Zeng Y, Huang C, Duan D, et al. Injectable temperature-sensitive hydrogel system incorporating deferoxamine-loaded microspheres promotes H-type blood vessel-related bone repair of a critical size femoral defect. *Acta biomaterialia*. 2022. doi:10.1016/j.actbio.2022.09.018
22. Feng P, Luo Y, Ke C, et al. Chitosan-Based Functional Materials for Skin Wound Repair: mechanisms and Applications. *Front Bioengineering Biotechnol*. 2021;9. doi:10.3389/fbioe.2021.650598
23. Iacob AT, Lupascu FG, Apotrosoaei M, et al. Recent Biomedical Approaches for Chitosan Based Materials as Dru Delivery Nanocarriers. *Pharmaceutics*. 2021;13(4):587. doi:10.3390/pharmaceutics13040587
24. Guo Y, Chen Y, Han P, et al. Biocompatible chitosan-carbon nanocage hybrids for sustained drug release and highly efficient laser and microwave co-irradiation induced cancer therapy. *Acta biomaterialia*. 2020;103:237–246. doi:10.1016/j.actbio.2019.12.010
25. Liu C, Yang P, Li J, Cao S, Shi J. NIR/pH-responsive chitosan hydrogels containing TiC/AuNRs with NIR-triggered photothermal effect. *Carbohydr Polym*. 2022. doi:10.1016/j.carbpol.2022.119853
26. Wasupalli GK, Verma D. Thermosensitive injectable hydrogel based on chitosan-polygalacturonic acid polyelectrolyte complexes for bone tissue engineering. *Carbohydr Polym*. 2022;294:119769. doi:10.1016/j.carbpol.2022.119769
27. Mei E, Chen C, Li C, et al. Injectable and Biodegradable Chitosan Hydrogel-Based Drug Depot Contributes to Synergistic Treatment of Tumors. *Biomacromolecules*. 2021;22(12):5339–5348. doi:10.1021/acs.biomac.1c01279
28. Shang T, Yu X, Han S, Yang B. Nanomedicine-based tumor photothermal therapy synergized immunotherapy. *Biomaterials sci*. 2020;8 (19):5241–5259. doi:10.1039/d0bm01158d
29. Zhao L, Zhang X, Wang X, Guan X, Zhang W, Ma J. Recent advances in selective photothermal therapy of tumor. *J Nanobiotechnology*. 2021;19 (1). doi:10.1186/s12951-021-01080-3
30. Huo J, Jia Q, Huang H, et al. Emerging photothermal-derived multimodal synergistic therapy in combating bacterial infections. *Chem Soc Rev*. 2021;50(15):8762–8789. doi:10.1039/d1cs00074h
31. Li X, Lovell JF, Yoon J, Chen X. Clinical development and potential of photothermal and photodynamic therapies for cancer. *Nat Rev Clin Oncol*. 2020;17(11):657–674. doi:10.1038/s41571-020-0410-2

32. Salimi M, Mosca S, Gardner B, Palombo F, Matousek P, Stone N. Nanoparticle-Mediated Photothermal Therapy Limitation in Clinical Applications Regarding Pain Management. *Nanomaterials*. 2022;12(6):6. doi:10.3390/nano12060922

33. Bianchi L, Mooney R, Cornejo YR, et al. Thermal analysis of laser irradiation-gold nanorod combinations at 808 nm, 940 nm, 975 nm and 1064 nm wavelengths in breast cancer model. *Int J Hyperthermia*. 2021;38(1):1099–1110. doi:10.1080/02656736.2021.1956601

34. Li Z, Lai X, Fu S, et al. Immunogenic Cell Death Activates the Tumor Immune Microenvironment to Boost the Immunotherapy Efficiency. *Adv Sci*. 2022. doi:10.1002/advs.202201734

35. Li Z, Zhou L, Qin Y, et al. Manganese doped polypyrrole nanoparticles for photothermal/chemodynamic therapy and immune activation. *Nanotechnology*. 2022. doi:10.1088/1361-6528/ac9739

36. Qiu Y, Wu Z, Chen Y, et al. Nano Ultrasound Contrast Agent for Synergistic Chemo-photothermal Therapy and Enhanced Immunotherapy Against Liver Cancer and Metastasis. *Adv Sci*. 2023. doi:10.1002/advs.202300878

37. Zhong L, Xia Y, He T, et al. Polymeric photothermal nanoplatform with the inhibition of aquaporin 3 for anti-metastasis therapy of breast cancer. *Acta biomaterialia*. 2022;153:505–517. doi:10.1016/j.actbio.2022.09.026

38. Mohan H, Fagan A, Giordani S. Carbon Nanomaterials (CNMs) in Cancer Therapy: a Database of CNM-Based Nanocarrier Systems. *Pharmaceutics*. 2023;15(5):1545. doi:10.3390/pharmaceutics15051545

39. Negri V, Pacheco-Torres J, Calle D, López-Larrubia P. CarbonR Nanotubes in Biomedicine. *Topics in Current Chem*. 2020. doi:10.1007/s41061-019-0278-8

40. Chen YW, Su YL, Hu SH, Chen SY. Functionalized graphene nanocomposites for enhancing photothermal therapy in tumor treatment. *Adv Drug Deliv Rev*. 2016;105:190–204. doi:10.1016/j.addr.2016.05.022

41. Tian Y, Yang P, Lin Y, et al. Assessment of Carbon Nanoparticle Suspension Lymphography-Guided Distal Gastrectomy for Gastric Cancer. *JAMA network open*. 2022;5(4):e227739. doi:10.1001/jamanetworkopen.2022.7739

42. Liu C, Xu P, Shao S, et al. Study on naked eye tracing of inguinal sentinel lymph nodes in penile cancer patients with carbon nanoparticle suspension injection. *Front med*. 2023. doi:10.3389/fmed.2023.1139986

43. Huang Y, Xie P, Yang ST, et al. Carbon nanoparticles suspension injection for the delivery of doxorubicin: comparable efficacy and reduced toxicity. *Mater Sci Eng C Mater Biol Appl*. 2018;92:416–423. doi:10.1016/j.msec.2018.07.012

44. Xie P, Yang ST, He T, Yang S, Tang XH. Bioaccumulation and Toxicity of Carbon Nanoparticles Suspension Injection in Intravenously Exposed Mice. *Int J Mol Sci*. 2017;18(12):12. doi:10.3390/ijms18122562

45. Xie P, Xin Q, Yang ST, et al. Skeleton labeled (13)C-carbon nanoparticles for the imaging and quantification in tumor drainage lymph nodes. *Int J Nanomedicine*. 2017;12:4891–4899. doi:10.2147/IJN.S134493

46. Tian Y, Lin Y, Guo H, et al. Safety and efficacy of carbon nanoparticle suspension injection and indocyanine green tracer-guided lymph node dissection during robotic distal gastrectomy in patients with gastric cancer. *Surg Endosc*. 2022;36(5):3209–3216. doi:10.1007/s00464-021-08630-8

47. Wu B, Wan J, Zhang Y, Pan B, Lo IMC. Selective Phosphate Removal from Water and Wastewater using Sorption: process Fundamentals and Removal Mechanisms. *Environ Sci Technol*. 2020;54(1):50–66. doi:10.1021/acs.est.9b05569

48. Zhao P, Zhang Y, Chen X, et al. Versatile Hydrogel Dressing with Skin Adaptiveness and Mild Photothermal Antibacterial Activity for Methicillin-Resistant Staphylococcus Aureus-Infected Dynamic Wound Healing. *Adv Sci*. 2023;10(11):e2206585. doi:10.1002/advs.202206585

49. Wang L, Chen S, Pei W, Huang B, Niu C. Magnetically targeted erythrocyte membrane coated nanosystem for synergistic photothermal/chemotherapy of cancer. *J Materials Chem B*. 2020. doi:10.1039/d0tb00364f

50. Wu F, Zhang M, Lu H, et al. Triple Stimuli-Responsive Magnetic Hollow Porous Carbon-Based Nanodrug Delivery System for Magnetic Resonance Imaging-Guided Synergistic Photothermal/Chemotherapy of Cancer. *ACS Appl Mater Interfaces*. 2018;10(26):21939–21949. doi:10.1021/acsami.8b07213

51. van Rhoon GC, Wust P. Introduction: non-invasive thermometry for thermotherapy. *Int J Hyperthermia*. 2005;21(6):489–495. doi:10.1080/02656730500272963

52. Babbs CF, DeWitt DP. Physical principles of local heat therapy for cancer. *Med Instrum*. 1981;15(6):367–373.